Brain Stimulation 12 (2019) 1159–1168

Contents lists available at ScienceDirect

Brain Stimulation

journal homepage: http://www.journals.elsevier.com/brain-stimulation

Towards precise brain stimulation: Is electric field simulation related to neuromodulation?

Daria Antonenko [a, b, *], Axel Thielscher [c, d], Guilherme Bicalho Saturnino [c, d], Semiha Aydin [e], Bernd Ittermann [e], Ulrike Grittner [f, g], Agnes Flöel [a, b, h, **]

[a] Charité – Universitätsmedizin Berlin, Corporate Member of Freie Universität Berlin, Humboldt-Universität zu Berlin, And Berlin Institute of Health, Department of Neurology, NeuroCure Clinical Research Center, Charitéplatz 1, 10117, Berlin, Germany
[b] Department of Neurology, Universitätsmedizin Greifswald, Ferdinand-Sauerbruch-Straße, 17475, Greifswald, Germany
[c] Danish Research Centre for Magnetic Resonance, Centre for Functional and Diagnostic Imaging and Research, Copenhagen University Hospital Hvidovre, Denmark
[d] Department of Electrical Engineering, Technical University of Denmark, Kgs Lyngby, Denmark
[e] Physikalisch-Technische Bundesanstalt (PTB), Abbestr. 2, 10587, Berlin, Germany
[f] Berlin Institute of Health (BIH), Anna-Louisa-Karsch-Straße 2, 10178, Berlin, Germany
[g] Charité – Universitätsmedizin Berlin, Corporate Member of Freie Universität Berlin, Humboldt-Universität zu Berlin, And Berlin Institute of Health, Institute of Biometry and Clinical Epidemiology, Charitéplatz 1, 10117, Berlin, Germany
[h] German Centre for Neurodegenerative Diseases (DZNE) Standort Greifswald, Greifswald, Germany

ARTICLE INFO

Article history:
Received 20 November 2018
Received in revised form
18 March 2019
Accepted 19 March 2019
Available online 22 March 2019

Keywords:
Transcranial direct current stimulation
Computational modeling
Magnetic resonance spectroscopy
GABA
Resting-state functional magnetic resonance imaging
Brain networks

ABSTRACT

Background: Recent research on neural and behavioral consequences of transcranial direct current stimulation (tDCS) has highlighted the impact of individual factors, such as brain anatomy which determines current field distribution and may thus significantly impact stimulation effects. Computational modeling approaches may significantly advance our understanding of such factors, but the association of simulation-based tDCS-induced fields and neurophysiological outcomes has not been investigated.
Objectives: To provide empirical evidence for the relationship between tDCS-induced neurophysiological outcomes and individually induced electric fields.
Methods: We applied tDCS during eyes-closed resting-state functional resonance imaging (rsfMRI) and assessed pre-post magnetic resonance spectroscopy (MRS) in 24 participants. We aimed to quantify effects of 15-min tDCS using the "classical" left SM1-right supraorbital area montage on sensorimotor network (SMN) strength and gamma-aminobutyric acid (GABA) and glutamate concentrations, implementing a cross-over counterbalanced design with three stimulation conditions. Additional structural anatomical MRI sequences and recordings of individual electrode configurations allowed individual electric field simulations based on realistic head models of all participants for both conditions.
Results: On a neurophysiological level, we observed the expected reduction of GABA concentrations and increase in SMN strength, both during anodal and cathodal compared to sham tDCS, replicating previous results. The magnitudes of neurophysiological modulations induced by tDCS were significantly associated with simulation-based electric field strengths within the targeted left precentral gyrus.
Conclusion: Our findings corroborate previous reports on tDCS-induced neurophysiological modulations and further advance the understanding of underlying mechanisms by providing first empirical evidence for the association of the injected electric field and neuromodulatory effects.

Introduction

With increasing use of transcranial direct current stimulation (tDCS) in experimental and clinical studies, research into individual factors determining tDCS effects is of particular importance [1,2]. Due to the heterogeneity of tDCS-induced effects between studies but also due to variability within samples, several research reports have focused on unveiling individual contributors to and predictors

* Corresponding author. Department of Neurology, Universitätsmedizin Greifswald, Ferdinand-Sauerbruch-Straße, 17475 Greifswald, Germany.
** Corresponding author. Department of Neurology, Universitätsmedizin Greifswald, Ferdinand-Sauerbruch-Straße, 17475 Greifswald, Germany.
E-mail addresses: daria.antonenko@uni-greifswald.de (D. Antonenko), agnes.floeel@uni-greifswald.de (A. Flöel).

https://doi.org/10.1016/j.brs.2019.03.072
1935-861X/

of the responsiveness to tDCS [3,4]. As such, various internal (related to the individual) and external variables (related to stimulation parameters, experimental setting and study design) have been suggested to affect the direction or magnitude of the tDCS-induced modulation of behavioral or neurophysiological outcomes [1].

Individual brain anatomy has been identified as a main determinant of current distribution, and therefore may be closely tied to quantifiable tDCS effects [5–8]. Therefore, anatomically accurate and individualized computational modeling of the electric field distribution might be useful to advance the understanding and optimization of non-invasive brain stimulation (NIBS)-induced effects [1,9,10]. Established simulation approaches rely on realistic three-dimensional head models of each individual that are reconstructed from structural MRI and include all major tissue classes, specific conductivity assumptions, and electrode properties [11–13].

Electric field simulations have been most frequently used for a qualitative visualization of the induced field patterns based on one or a few exemplary head models. However, to date, only few studies have related model predictions to neurophysiological and individual behavioral outcomes of NIBS across groups of subjects [7,14,15]. For instance, using transcranial alternating current stimulation (tACS) of different frequencies and with different electrode montages, correlational relationships of mean electric field strengths and magnitude of changes in low frequency fluctuations were observed [14]. Using tDCS over left dorsolateral prefrontal cortex, Kim et al. [7] provided preliminary evidence for a positive correlation of the magnitude of simulated current density values and improvements in verbal working memory performance. However, it is not clear yet whether the amount of current delivered to a particular brain area in the individual brain is related to tDCS-induced neurochemical and functional network modulations.

In the present study, we therefore investigated the relationship between tDCS-induced neurophysiological modulations and simulation-based individual electric field properties. For that, we simulated the actual electrode configurations in each condition for each participant individually. We used the “classical” electrode montage to modulate sensorimotor networks (i.e., left SM1-right supraorbital area montage). Evidence for the efficiency of this tDCS montage and direction of induced effects has accumulated in various research studies using different methodological approaches [16–20]. Effects of anodal, cathodal and sham tDCS were assessed on simultaneously acquired resting-state functional resonance imaging (rsfMRI) functional connectivity and on changes in gamma-aminobutyric and glutamatergic metabolite levels using magnetic resonance spectroscopy. In addition, we acquired anatomical sequences optimized for realistic head modeling for each participant in each condition, in order to evaluate the link between subject-specific electric field strengths within the targeted left precentral gyrus and tDCS-induced neurophysiological modulations. Based on previous research, we hypothesized that in active tDCS conditions, overall metabolite concentration in the sensorimotor cortex would decrease, and functional connectivity would increase [16,21–24]. Further, we hypothesized that inter-individual differences in the tDCS-induced electric field within the targeted precentral gyrus would be correlated with individual differences in the magnitude of neurophysiological modulations.

Material and methods

Participants and procedure

Twenty-four young adults (12 women, mean/SD age: 25/4) participated in the experiment. For characteristics of the study sample, see Supplementary Methods. All subjects participated in three sessions where either anodal (atDCS), cathodal (ctDCS) or sham tDCS (stDCS) was applied for 15 min during resting-state fMRI, see Fig. 1. The order of stimulation conditions was counterbalanced across subjects, and sessions were separated by one week. In each session, MRS measurement was acquired before and after the 15-min tDCS interval [see 16].

tDCS

Direct current stimulation was delivered through a battery-driven MRI-compatible stimulator (neuroConn DC-Stimulator Plus, neuroCare Group GmbH, Munich, Germany) positioned outside the scanner room, using saline-soaked sponges. Two filter boxes, absorbing radio frequency noise, were placed between stimulator and electrodes inside and outside the scanner room and 5-kOhm resistors were included in each electrode cable. This setting has been previously used in our group [16,25,26]. The “active” electrode ($5 \times 7\ cm^2$) was centered over left SM1 (C3 according to 10–20 EEG system), the reference electrode ($10 \times 10\ cm^2$) was positioned over the right supraorbital region. Electrode placements were verified both on the localizer scan in the beginning of MRI assessment and on each individual T1-weighted image after scanning. In the atDCS and ctDCS conditions, stimulation was delivered continuously for 15 min (with 10 s fade in/out intervals) with a constant current of 1 mA. In the stDCS condition, stimulation was turned off after 30 s. Mood ratings [27] and an adverse events questionnaire were administered [adapted from 28] (see Supplementary Material and Results).

Electrode impedances were continuously monitored. Mean (SD) impedance across sessions was 15.97 (0.85) kΩ with no difference between stimulation conditions (atDCS: 16.02 (0.77), ctDCS: 15.87 (0.96), paired sample t-test: $t(23) = 0.72$, $p = 0.478$). Intra-individual impedance variability during a stimulation session was low, ranging from 0 to 3 kΩ with no difference between stimulation conditions either (atDCS: 0.96 (0.68), ctDCS: 0.91 (0.95), paired sample t-test: $t(23) = 0.21$, $p = 0.838$).

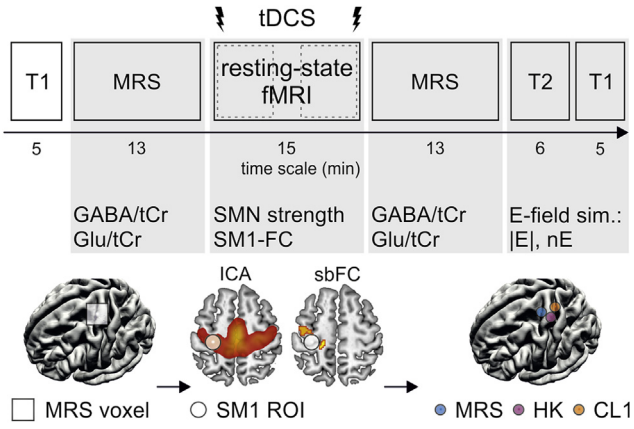

Fig. 1. Upper panel: Illustration of experimental design. Order and length of MRI sequences are shown. During resting-state fMRI, tDCS was applied (anodal, cathodal, and sham condition for each participant in separate sessions with counterbalanced order). Lower panel: Dependent variables quantified from respective MRI sequences and illustrative regions-of-interests (ROIs) positions during MRS, in resting-state fMRI analysis and for extraction of electrical field strengths. MRS, magnetic resonance spectroscopy. GABA, gamma-aminobutyric acid, Glu, glutamate. tCr, total creatine. tDCS, transcranial direct current stimulation. fMRI, functional magnetic resonance imaging. SMN, sensorimotor network. SM1, primary sensorimotor cortex. FC, functional connectivity. E-field sim., electric field simulation. ICA, independent component analysis. sbFC, seed-based functional connectivity. HK, gyral crown of the hand knob. CL1, network cluster ROI.

MRI acquisition

MR images and spectra were acquired on a 3-T Siemens Verio scanner (Siemens Healthcare, Erlangen, Germany) using a 32-channel head coil. After recording of a scout image, high-resolution anatomical images were acquired using a three-dimensional T1-weighted magnetization prepared gradient-echo sequence (MPRAGE) with repetition time (TR) = 2300 ms, echo time (TE) = 3.03 ms, inversion time (TI) = 900 ms, flip angle = 9°, 256 × 256 × 192 matrix, 1 mm^3 isotropic voxel. This image was used to place the spectroscopic voxel of interest (22 × 22 × 22 mm^3) over the left precentral gyrus hand knob [29]. For MRS, first the transmitter radiofrequency voltage was calibrated for the individual volume of interest, followed by adjustment of all first- and second-order shims using FAST(EST)MAP [30,31]. Gamma-aminobutyric acid (GABA)-edited spectra were recorded using the MEGA-PRESS technique [32,33], see Supplementary Methods for further details. Acquisition of resting-state fMRI was performed using two consecutive echo-planar imaging (EPI) sequences (3 × 3 × 4 mm^3; TR 2300 ms; TE 30 ms; flip angle 90°; 35 slices; no gap; interleaved acquisition; field of view 192 × 192 mm^2; 64 × 64 matrix; 150 vol). Subjects were instructed to keep their eyes closed, try not to fall asleep and to think of nothing particular. None of the participants had fallen asleep during the stimulation interval as evinced from oral interview after scanning.

In order to create accurate individualized head models for finite element method (FEM)-based electric field simulations, we acquired additional T1- (1 × 1 × 1 mm^3, TR 2300 ms, TE 2.96 ms, TI 900 ms, flip angle 9°; using selective water excitation for fat suppression) and T2-weighted (1 × 1 × 1 mm^3, TR 12770 ms, TE 86 ms, flip angle 111°) anatomical images at the end of the sham stimulation session for each individual.

MRI analysis

MRS. Edited spectra were analyzed using LCModel [34] with a measured basis set containing GABA, N-acetylaspartate (NAA), glutamate (Glu), glutamine, and glutathione and referenced to the concentrations used for creating the basis set. For fitting of the unedited spectrum, a simulated basis set containing 16 metabolites was used (i.e., alanine, aspartate, phosphocholine, creatine, phosphocreatine, GABA, Glu, glutamine, myo-inositol, lactate, NAA, scyllo-inositol, taurine, glucose, N-acetylaspartylglutamate, and glycerophosphocholine). GABA and Glu concentration was quantified as ratio to total creatine (tCr) fitted from the unedited spectra [35,36]. Four (out of 72) datasets were excluded from subsequent analysis of GABA/tCr change and three datasets were excluded from analysis of Glu/tCr change due to problems with MEGA-PRESS during MRS acquisition, incorrect voxel positioning or Cramér-Rao lower bounds above the threshold of 30%.

Resting-state fMRI. Functional connectivity analysis was performed using the Matlab-based CONN toolbox version 17f (www.nitrc.org/projects/conn) [37]. Default preprocessing steps were applied on individual datasets including functional realignment, slice-time correction, structural segmentation and normalization to the MNI template, functional segmentation and normalization, and smoothing (with a 6-mm Gaussian kernel). Physiological and other spurious sources of noise were estimated and regressed out using a combination of the anatomical component-based noise correction (CompCor) method (5 white matter and 5 CSF regressors), scrubbing (invalid scans as regressors), motion regression (12 regressors: 6 motion parameters and 6 first-order derivates), and filtering, implemented in CONN [38]. High-pass temporal filtering at 0.01 Hz was applied on functional data. Head motion was corrected using the artefact detection method (www.nitrc.org/projects/artifact_detect/) implemented in CONN. Three datasets (two in anodal condition, one in sham condition) were excluded from further analyses due to severe motion artefacts. A region-of-interest (ROI) was defined as an 8-mm sphere around the mean center coordinates of MRS voxel positions in the left precentral gyrus (x = −30, y = −15, z = 48). First-level analyses included calculation of individual whole-brain seed-to-voxel functional connectivity maps (using the MRS ROI as a seed and correlating its filtered and motion-corrected blood oxygenation level-dependent time course with the time course of all other voxels in the brain) and decomposition of the dataset in 20 independent factors (components) using independent component analysis (ICA).

For second-level analysis, Pearson's *r* correlation coefficients were transformed to normally distributed *z* scores using Fisher's *r*-to-*z* transformation. Whole-brain seed-based functional connectivity maps were then compared between stimulation conditions using separate paired t-tests for atDCS, and ctDCS condition, respectively, compared to stDCS. In group-level comparisons, reported clusters were thresholded at $p_{FDR}<0.05$ using a cluster-forming threshold of $p_{uncor}<0.005$.

After group-level ICA for estimation of 20 independent spatial components, individual subject-level spatial map estimation was performed using back-reconstruction of group-level ICs into single subject maps for each condition [39–41]. The component of interest was selected from ICA-based analysis by computing the spatial correlation between each group-level spatial map with CONN's network masks (correlation coefficient: r = 0.51 of the IC that best matched, i.e., showed the highest correlation, to the CONN template of the sensorimotor network). Individual subject- and condition-specific sensorimotor network (SMN) components, as derived from the backprojection step in the ICA, were then masked by the precentral gyrus (MRS) ROI, and the mean signal intensity was extracted to quantify functional individual SMN strengths of each subject in each stimulation condition [16,21,22].

Simulation of electrical fields

The software SimNIBS 2.0 was used to calculate the electric field induced by tDCS based on the finite element method (FEM) and individualized head models derived from the structural MR images (www.simnibs.org) [42,43]. First, T1-and T2-weighted anatomical images were used to create individualized tetrahedral FE head meshes for the sham condition of each subject, using integrated tools from FreeSurfer (https://surfer.nmr.mgh.harvard.edu), FMRIB's FSL (https://fsl.fmrib.ox.ac.uk/fsl/fslwiki), MeshFix [44], and Gmsh [45].

Electrode positions (i.e., the center coordinates and orientations of the modeled electrodes) for each of the two stimulation sessions were precisely placed on the head mesh by visual inspection of the structural T1 images acquired at each session start, using the render view of MRICron (https://www.nitrc.org/projects/mricron). The positions were additionally verified with individual photographs taken during all intra-scanner tDCS application sessions. These steps were repeated separately for the atDCS and for the ctDCS sessions. Then, electric field simulations were computed for atDCS and ctDCS conditions for the “active” electrode over left SM1 and the reference electrode over right supraorbital cortex. As the size of the reference electrode's sponge led to a small part of the vertical side protruding from the forehead, the area of the electrode that actually touched the forehead was measured individually during each experimental session and modeled accordingly (i.e., the size of the “active” electrodes was always set to 5 × 7 cm^2; the width of the “reference” electrode was 10 cm, while the individual values for its length varied between 7.9 and 8.8 cm; electrode thickness: 2 mm; sponge thickness: 3 mm). Connector positions were defined in

relation to the electrode center of the "active" electrode (0.0 cm, −3.0 cm; on the front side), and of the reference electrode (−3.0 cm, 0.0 cm; on the top side), respectively, with a size of 1 cm^2. Conductivity values were set as follows: σ(white matter) = 0.126 S/m, σ(grey matter) = 0.275 S/m, σ(cerebrospinal fluid) = 1.654 S/m, σ(bone) = 0.010 S/m, σ(scalp) = 0.465, σ(spongy bone) = 0.010 S/m, σ(compact bone) = 0.008 S/m, σ(eye balls) = 0.500 S/m, σ(eye region) = 0.250 S/m, σ(electrode rubber) = 29 S/m, σ(electrode saline) = 1.5 S/m [13,46]. After the field calculations, the middle layer of the cortical sheet was estimated from the pial and white matter surfaces provided by FreeSurfer. The electric field strength (i.e., the vector norm of the electric field E) and the field component orthogonal to the cortical sheet were extracted at the middle layer of the cortex [15]. The individual results were transformed to the average surface 'fsaverage' provided by Freesurfer, and group averages and standard deviations of the electric field strength and the normal component were calculated for each stimulation condition.

In order to test our hypothesis that inter-individual differences in the electric field induced within the left precentral gyrus were related to differences in the observed neurophysiological modulations, we extracted the individual fields from 4-mm diameter spheres at three regions-of-interest (ROI). The first ROI was determined at the position on the fsaverage template closest to the center of the MRS voxel (MRS; x = −30, y = −15, z = 48). The second ROI was set on the crown of the precentral gyrus at the center of the handknob in medial-lateral direction (HK; x = −41, y = −12, z = 65). We chose this second ROI as it experienced, on average, the highest field strength in the primary motor region. The third ROI within the precentral gyrus was selected based on tDCS-induced functional network effects obtained from seed-based resting-state fMRI analysis (see Results section, CL1; x = −18, y = −30, z = 56). For all ROIs, both the electric field strength and the normal component of the field were extracted and analyzed separately to test for correlations with tDCS-induced neurophysiological modulations in metabolite concentrations and functional coupling in SMN. The normal component is traditionally seen as the main field component causing physiological effects [47], but this view is questioned by more recent findings as being too simplistic [48]. We thus opted for testing both the field strength and the normal component here.

Statistical analysis

IBM SPSS Statistics 24 (http://www-01.ibm.com/software/uk/analytics/spss/) was used for statistical analyses. In order to determine stimulation condition effects, linear mixed models (random intercept models) [49] were calculated for each dependent variable to adjust for the dependency of repeated measures within individuals. Models included repeated measurements (condition: atDCS, ctDCS, stDCS) as level-one units nested in individuals who were level-two units (which corresponded to random effects). Model-based post hoc pairwise comparisons of estimated fixed effects were computed. Difference in adverse effects between conditions was analyzed with logistic mixed model analysis, adjusted for sex. Spearman's rank correlation coefficients (r_S) were computed as association measures between neurophysiological effects and modeling-based electric field strengths. No adjustment for multiple testing was applied. A two-sided significance level of $\alpha = 0.05$ was used.

Results

tDCS effects on metabolite concentrations

Precentral gyrus GABA change differed significantly between conditions ($F(2,43) = 3.642$, $p = 0.035$; N = 24/68 data points; Fig. 2). Post hoc comparisons revealed that precentral gyrus GABA was reduced after atDCS compared to stDCS (mean difference: −0.19, 95%–CI: −0.35, −0.03; $p = 0.018$) and after ctDCS compared to stDCS (mean difference: −0.17, 95%–CI: −0.33, −0.02; $p = 0.032$) with no difference between atDCS and ctDCS (mean difference: −0.02, 95%–CI: −0.18, 0.13, p = 0.778). Similarly, precentral gyrus Glu change differed significantly between conditions ($F(2,66) = 3.165$, $p = 0.049$; N = 24/69 data points; Fig. 2). Here, post hoc comparisons revealed that Glu was reduced after ctDCS

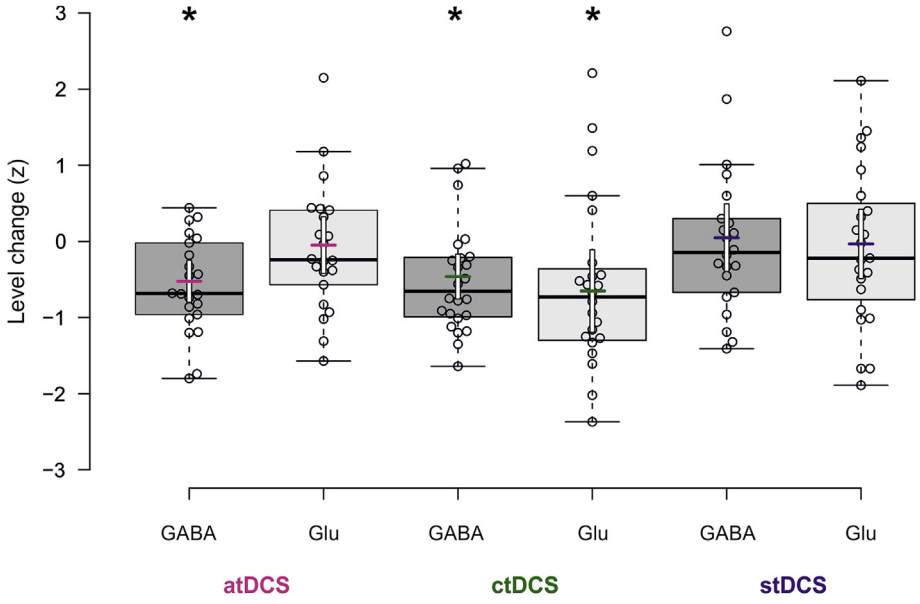

Fig. 2. Change of metabolite concentration after the stimulation interval. GABA and Glu level changes are given as ratios to tCr normalized to the sham stimulation condition (*z*-values). GABA, gamma-aminobutyric acid; Glu, Glutamate. atDCS, anodal transcranial direct current stimulation; ctDCS, cathodal direct current stimulation; stDCS, sham transcranial direct current stimulation. Means (colored short lines) and 95% confidence intervals (white bars) are shown over individual data points and box plots. Graphs created with BoxPlotR (http://boxplot.tyerslab.com/) [61]. *$p \leq 0.05$.

compared to stDCS (mean difference: −0.05, 95%−CI: −0.096, −0.005; $p = 0.030$) and ctDCS compared to atDCS (mean difference: −0.05, 95%−CI: −0.093, −0.003; $p = 0.038$) with no difference between atDCS and stDCS (mean difference: −0.003, 95% CI: −0.05, 0.04, p = 0.908).

tDCS effects on seed-based functional connectivity

Voxel-wise comparison of the correlation between the mean BOLD time course within the left precentral gyrus with all other brain voxels revealed significantly increased functional connectivity during atDCS, and ctDCS, respectively, compared to stDCS. During atDCS, functional connectivity was increased between the seed and clusters within the left precentral gyrus as well as between the seed and the right frontal orbital cortex and superior frontal gyrus. During ctDCS, functional connectivity was increased between the seed and the intracalcarine cortex and in the postcentral gyrus (Fig. 3, Table 1).

tDCS effects on SMN strength

SMN strengths differed significantly between conditions ($F(2,113) = 4.911$, $p = 0.009$; N = 24/138 data points; Fig. 4). Post hoc comparisons revealed augmented SMN strength during atDCS compared to stDCS (mean difference: 0.39, 95%−CI: 0.13, 0.65; $p = 0.004$) and ctDCS compared to stDCS (mean difference: 0.31, 95%−CI: 0.05, 0.56, $p = 0.018$) with no difference between atDCS and ctDCS (mean difference: 0.08, 95%−CI: −0.18, 0.34, p = 0.53).

Individually modeled electric fields

As expected, maximum modeled field intensities were induced between the two electrodes with high intensities around the targeted precentral gyrus during anodal stimulation (see Fig. 5A and

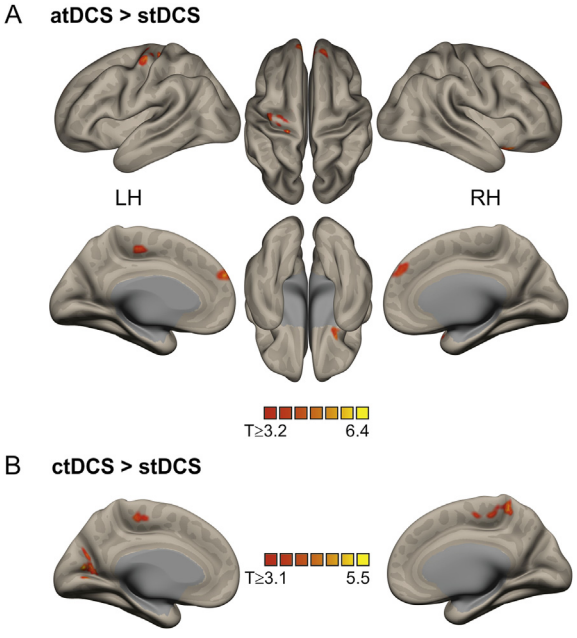

Fig. 3. Seed-based functional connectivity during atDCS compared to stDCS condition with seed in left precentral gyrus. Clusters in red-yellow depict increased correlations in atDCS. Cluster-extent thresholds were calculated in CONN, resulting in $k = 94$ for $p_u < 0.005$ which corresponds to $p_{FDR} < 0.05$ (false-discovery rate correction for multiple comparisons). atDCS, anodal transcranial direct current stimulation; ctDCS, cathodal direct current stimulation; stDCS, sham transcranial direct current stimulation. LH, left hemisphere; RH, right hemisphere. (For interpretation of the references to color in this figure legend, the reader is referred to the Web version of this article.)

Table 1
Comparison of seed-based functional connectivity between stimulation conditions.

Brain region	Coordinates			*k*	T
	x	y	z		
atDCS > stDCS					
Precentral Gyrus	−18	−30	56	107	6.35
Frontal Orbital Cortex	32	16	−22	94	6.21
Superior Frontal Gyrus	−2	56	30	240	5.89
Precentral Gyrus	−40	−18	60	237	5.27
ctDCS > stDCS					
Intracalcarine Cortex	−6	−70	8	164	5.50
Postcentral Gyrus	14	−42	62	204	5.23

Anatomical location of cluster peaks, FDR-corrected ($p_{FDR} < 0.05$, $k > 94$ for atDCS versus stDCS; $p_{FDR} < 0.05$, $k > 164$ for ctDCS versus sham). Coordinates of peak voxel (x, y, z in mm) in MNI space. *k*, cluster extent (number of voxels); T, t-value of peak voxel.

Fig. 5B for mean and standard deviations of the electric field strength). A different pattern occurred for the component of the electric field vector normal (i.e., orthogonal) to the cortical sheet (Fig. 5C), which peaked at left-hemispheric sensorimotor cortex, including the precentral and postcentral gyri with maximum intensity in the central sulcus. A very similar pattern emerged for the field distribution during cathodal stimulation (see Supplementary Fig. S1). Individual maps show the pattern for each of the 24 participants (for anodal: electric field strength, Supplementary Fig. S2, and normal component, Supplementary Fig. S3; for cathodal: electric field strength, Supplementary Fig. S4, and normal component, Supplementary Fig. S5).

Electric field strengths and normal components of the electric field extracted from the three ROIs are shown in Fig. 6 for both stimulation conditions. In atDCS (Fig. 6A), the electric field strength differed significantly between ROIs ($F(2,46) = 19.475$, $p < 0.001$; N = 24/72 data points). Post hoc comparisons revealed that the modeled field strength was higher at the network cluster (CL1) compared to the MRS voxel (mean difference: 0.030, 95%−CI: 0.017, 0.044; $p < 0.001$), and at the superficial handknob (HK) ROI compared to the MRS voxel (mean difference: 0.040, 95%−CI: 0.026, 0.053; $p < 0.001$). Similarly, the normal component of the field differed significantly between ROIs ($F(2,46) = 75.857$, $p < 0.001$). Post hoc comparisons revealed that the normal component was higher at CL1 compared to MRS (mean difference: 0.125, 95%−CI: 0.105, 0.146; $p < 0.001$) and HK (mean difference: 0.056, 95%−CI: 0.035, 0.076; $p < 0.001$), and at HK compared to MRS voxel (mean difference: 0.070, 95%−CI: 0.049, 0.090; $p < 0.001$).

In ctDCS (Fig. 6B), the electric field strength differed significantly between ROIs ($F(2,46) = 21.002$, $p < 0.001$; N = 24/72 data points). Post hoc comparisons revealed that the modeled field strength was higher at CL1 compared to MRS voxel (mean difference: 0.028, 95%−CI: 0.017, 0.040; $p < 0.001$), and at HK compared to MRS voxel (mean difference: 0.034, 95%−CI: 0.023, 0.046; $p < 0.001$). Similarly, the normal component of the modeled field differed significantly between ROIs ($F(2,69) = 59.568$, $p < 0.001$). Post hoc comparisons revealed that the normal component was more negative at CL1 compared to MRS (mean difference: −0.113, 95% −CI: −0.134, −0.092; $p < 0.001$) and HK (mean difference: −0.050, 95%−CI: −0.071, −0.029; $p < 0.001$), and at HK compared to MRS (mean difference: −0.063, 95%−CI: −0.084, −0.042; $p < 0.001$).

Modeling-based field strengths were correlated between atDCS and ctDCS conditions in all three ROIs (see Supplements and Supplementary Fig. S6). A significant correlation between the normal field components induced during atDCS versus ctDCS was only observed in the in HK. Lack of significant correlations in the two other ROIs indicates that differing electrode positions across the two simulations could potentially cause intra-individual variations in the spatial electric field patterns.

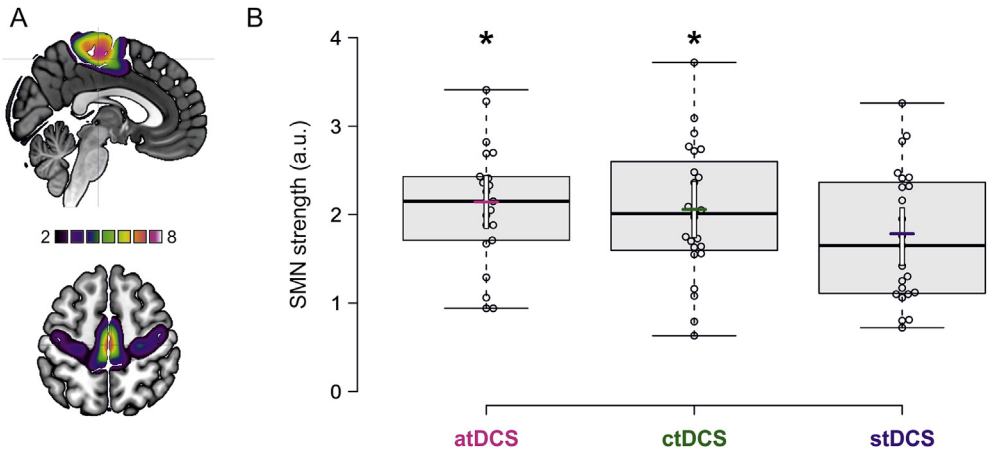

Fig. 4. A: Sensorimotor network derived from independent component analysis. B: Functional coupling in the SMN during stimulation (arbitrary units). SMN, sensorimotor network. atDCS, anodal transcranial direct current stimulation; ctDCS, cathodal direct current stimulation; stDCS, sham transcranial direct current stimulation. Means (colored short lines) and 95% confidence intervals (white bars) are shown over individual data points and box plots. Graphs created with BoxPlotR (http://boxplot.tyerslab.com/) [61]. *$p \leq 0.05$.

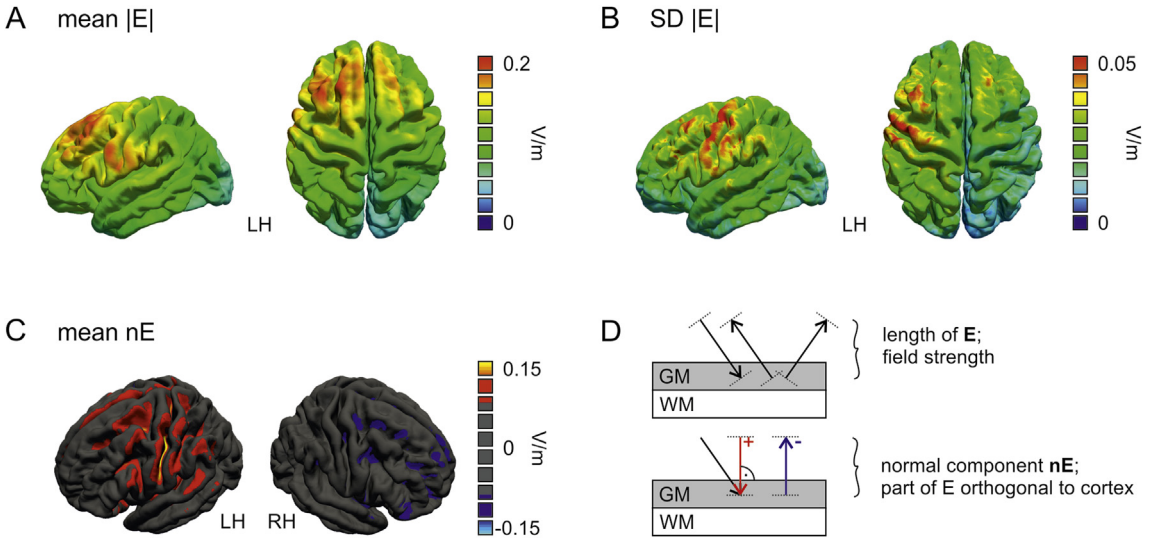

Fig. 5. Electric field distribution for the anodal tDCS condition, derived from FEM calculations using SimNIBS. A: Electric field strength (|E|) averaged across all participants. B: Variability of the electric field strength (standard deviation, SD). C: Component of the electric field strength that is directed orthogonally to the cortical sheet (termed "normal" component, nE). Positive values (red-yellow) indicate anodal stimulation, negative values (violet-blue) indicate cathodal stimulation. D: Schematic illustration of the electric field strength (i.e., length of vector E; black arrows) and the normal component (i.e., part of E orthogonal to the cortex; the red arrow entering the cortex denotes anodal stimulation, the blue arrow exiting the cortex denotes cathodal stimulation). GM, grey matter; WM, white matter. LH, left hemisphere. RH, right hemisphere. (For interpretation of the references to color in this figure legend, the reader is referred to the Web version of this article.)

Association between tDCS-induced neurophysiological changes and induced electric field as derived by electric field modeling

Magnitude of individual tDCS-induced GABA modulation was positively associated with the simulated electric fields within the precentral gyrus in atDCS (field strength: CL1: $r_S = 0.53$, $p = 0.013$; normal component: $r_S = 0.47$, $p = 0.032$; Fig. 7) and in ctDCS (field strength: MRS: $r_S = 0.45$, $p = 0.027$; HK: $r_S = 0.42$, $p = 0.039$; CL1: $r_S = 0.43$, $p = 0.037$; Fig. 8). Individual tDCS-induced modulation of SMN strength also correlated with electric fields in atDCS (normal component: CL1: $r_S = 0.53$, $p = 0.015$) and ctDCS (field strength: MRS: $r_S = -0.49$, $p = 0.017$; HK: $r_S = -0.43$, $p = 0.043$; note that here, correlation coefficients were negative, indicating an inverse relationship, i.e., individuals with higher induced field strengths showed a connectivity decrease during cathodal stimulation while those with low induced field strengths showed a connectivity increase).

Discussion

The present study aimed to relate neurophysiological modulations induced by tDCS assessed with MRS and rsfMRI to the induced electric field distributions within the targeted left precentral gyrus as estimated by numerical simulations. We conducted a systematic experiment using the "classical" SM1-SO electrode montage with rsfMRI during tDCS and pre-post MRS assessment in order to quantify neurophysiological effects in the left sensorimotor cortex. Further, we conducted electric field simulations using individual FEM-based head models in order to assess whether inter-individual differences in the neurophysiological modulations were related to different field intensities in selected cortical precentral ROIs.

On a neurophysiological level, we found reduced precentral gyrus GABA after atDCS and ctDCS, replicating previous findings [16,21–23,50]. Evidence from animal and human studies suggests that decrease in local GABA-mediated inhibition facilitates long-

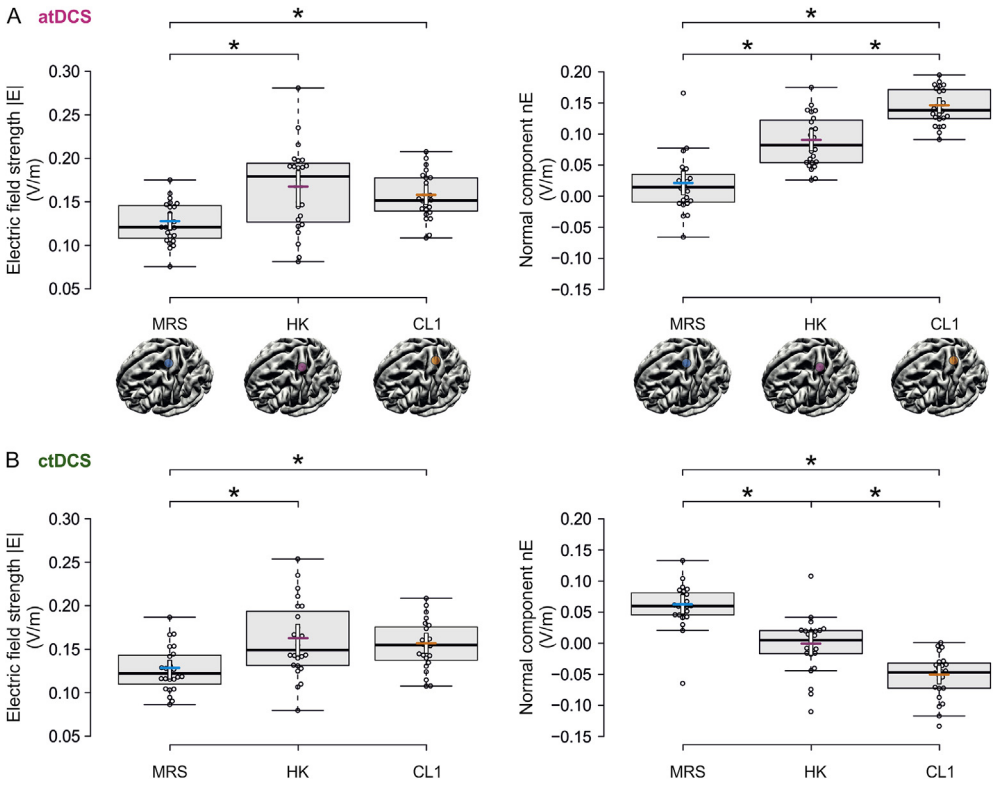

Fig. 6. Electric field strength and normal component (in V/m) extracted from the ROIs in MRS voxel, handknob and the cluster showing significant tDCS-induced modulation for atDCS (A) and ctDCS conditions (B). Means (colored short lines) and 95% confidence intervals (white bars) are shown over individual data points and box plots. Graphs created with BoxPlotR (http://boxplot.tyerslab.com/) [61]. MRS, magnetic resonance imaging voxel. HK, gyral crown of the handknob. CL1, significant cluster within the precentral gyrus (atDCS > stDCS; derived from resting-state analysis; note that for the ctDCS > stDCS contrast no cluster in the vicinity of the active electrode remained significant). atDCS, anodal transcranial direct current stimulation; ctDCS, cathodal direct current stimulation; stDCS, sham transcranial direct current stimulation. $^{*}p \leq 0.05$.

term potentiation-like activity and promotes unmasking of cortical horizontal connections [35,51–54]. Thus, reduced precentral gyrus GABA due to tDCS most likely reflected synaptic preserved plasticity in the underlying sensorimotor cortex, with parallel glutamatergic modulation determining increase or decrease in cortical excitability due to atDCS or ctDCS, respectively [23]. With regard to rsfMRI network modulation, tDCS induced functional connectivity increases within the targeted SMN, likewise corroborating previous findings [21,55,56]. In line with previous evidence, we observed strongest local effects, i.e., increased functional connectivity, in the vicinity of the precentral gyrus under the active electrode due to atDCS.

On the computational modeling level, we simulated individual electrode configurations separately for the atDCS and ctDCS conditions. The simulations suggest intra-individual differences in the injected fields for the two sessions (i.e., small variations in electrode positions produced variations in the electric fields in the selected ROIs). In line with [57], our findings show that carefully defining the electrode positions is important to ensure accurate results for field simulations. The variations were larger for the normal component of the field than for the field strength, possibly due to the fact that the normal component is also sensitive to changes of the field direction and not only its magnitude, given the rapidly changing orientation of the cortical sheet.

Our results support the hypothesis that individual electric field distribution, influenced by individual brain and head anatomy [10,46], is a key determinant of the neurophysiological effects evoked by tDCS. For atDCS, both GABA and functional connectivity modulations showed positive relationships with individually induced electric fields in CL1, indicating that higher field strengths were linked to increases in local plasticity. For ctDCS, GABA modulation showed a positive association in all three precentral ROIs, further sustaining the linkage between individually induced fields and local cortical plasticity. Functional connectivity modulation pointed towards a negative relationship, probably indicating non-monotonic dose effects of ctDCS, given that participants with highest field strengths exhibited reduced ctDCS-induced connectivity (compared to sham) while those with lower field strengths showed a connectivity increase. These results may account for higher variability of neurophysiological effects of ctDCS to atDCS in this study and others [58], potentially explaining the inconsistency of empirical findings with regard to ctDCS.

Significant correlations were observed in CL1 for atDCS and in all three precentral ROIs for ctDCS. This difference might at least in part stem from the slightly larger inter-individual spread of neurophysiological effects in the ctDCS condition, which might have increased power of the correlation analysis. In addition, the large inter-individual anatomical differences of the handknob area likely resulted in higher spatial variability of the electric fields and also of the non-linear registration to the fsaverage template in superficial brain areas compared to the fundus of the central sulcus. In combination, these methodological factors might have biased the results for atDCS towards the sulcal CL1 ROI.

The fact that the normal component is also sensitive to changes of the field direction contributes to our finding that significant correlations with the neurophysiological parameters mostly occurred for the field strength rather than for the normal component. The fsaverage template represents only coarse anatomical features and, caused by the inter-individual variability in cortical folding, individual cortical positions with varying orientations get mapped onto a common position on the fsaverage template. This effect created additional variability in the normal component, so

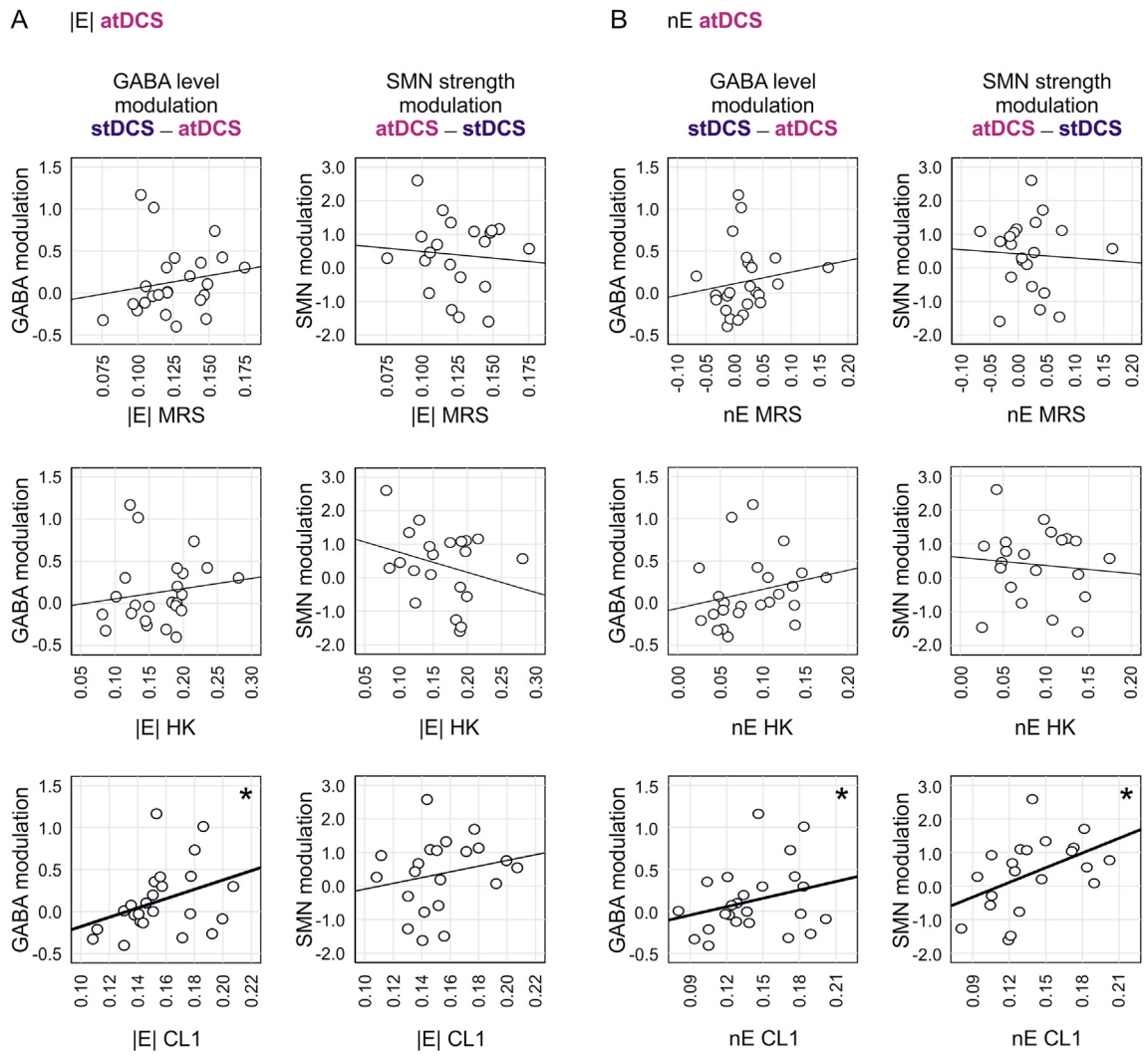

Fig. 7. Scatterplots of individual electric fields extracted from the ROIs (MRS voxel, gyral crown of the handknob, network cluster) with atDCS-induced neurophysiological modulation for GABAtCr and SMN functional coupling. A: Correlations of GABA and SMN strength modulation with electric field strengths |E|. B: Correlations with the normal component nE of the electric field. MRS, magnetic resonance imaging voxel. HK, gyral crown of the handknob. CL1, significant cluster within the precentral gyrus (atDCS > stDCS; derived from resting-state analysis). atDCS, anodal transcranial direct current stimulation; stDCS, sham transcranial direct current stimulation. $^{*}p < 0.05$.

that changes of the latter were not correlated with inter-individual variations in neurophysiological parameters anymore. Interestingly, the exception was the CL1 ROI in the fundus of the central sulcus, i.e., at a position where the alignment of the individual cortical surfaces to the template was most likely reliable. As a consequence, our approach seemed to be better suited to demonstrate inter-individual correlations with neurophysiological parameters for the electric field strength rather the normal component, even though the latter is often suggested to be the predominant part of the electric field causing physiological effects.

Only few studies have established a link between individual simulation-based electric fields and empirically assessed brain stimulation effects. Using tACS, Cabral-Calderin and colleagues found that for some stimulation conditions, mean electric field strength predicted local connectivity modulations. For example, the authors observed higher field strengths to be associated with increases and decreases in tACS-induced low frequency fluctuations [14]. Using transcranial magnetic stimulation (TMS), Mikkonen et al. observed a correlation of electric fields induced by tDCS with resting motor thresholds that was specific to the hand area of primary motor cortex, indicating higher induced fields in individuals with lower TMS motor thresholds [59]. Our data take these preliminary individual computational modeling approaches a step further, by providing first evidence for a relationship between simulation-based induced fields and local plasticity at the cortex targeted with brain stimulation.

Conclusions and outlook

In sum, our results suggest a linkage between modeled electric fields and neurophysiological effects of tDCS, both for GABAergic plasticity assessed by MRS and functional coupling assessed by resting-state fMRI. Our data emphasize the impact of individual brain anatomy on the injected field distribution, highlight the importance to consider inter-individual anatomical variability, and support the usefulness of numerical estimations of the electric field to make predictions about empirical effects. While further studies are needed to strengthen this link, these model predictions are an important complement to invasive or MR-based measurements of the induced electric field that directly validate the field estimates of simulation approaches [8,57,60]. In addition, while our study focused on the link between the electric field and the neurophysiological effects of tDCS over the left precentral gyrus, it should be acknowledged that tDCS with large pad electrodes as employed

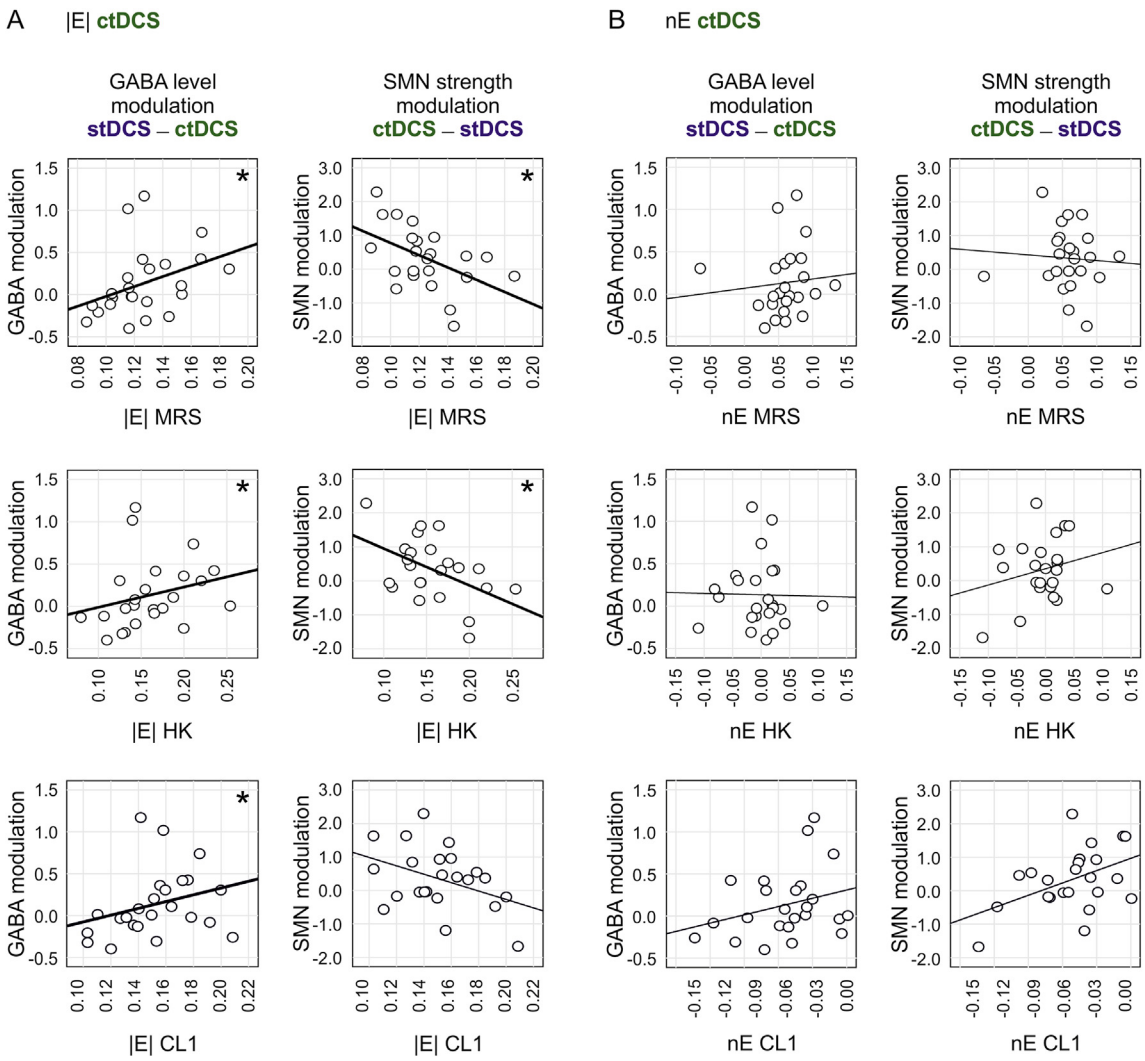

Fig. 8. Scatterplots of individual electric fields extracted from the ROIs (MRS voxel, handknob, network cluster) with ctDCS-induced neurophysiological modulation for GABAtCr and SMN functional coupling. A: Correlations of GABA and SMN strength modulation with electric field strengths |E|. B: Correlations with normal component nE of the electric field. MRS, magnetic resonance imaging voxel. HK, gyral crown of the handknob. CL1, significant cluster within the precentral gyrus (atDCS > stDCS; derived from resting-state analysis; note that for the ctDCS > stDCS contrast no cluster in the vicinity of the active electrode remained significant). atDCS, anodal transcranial direct current stimulation; ctDCS, cathodal direct current stimulation; stDCS, sham transcranial direct current stimulation. *$p < 0.05$.

here produces diffuse electric fields in extended areas of the brain. Future studies should thus test whether taking into account the combined field acting on several nodes of involved brain networks explains the neurophysiological effects of tDCS better than considering only a single, albeit important network node.

In the long run, modeling studies should aim to prospectively provide the experimenter with stimulation parameters, e.g., electric field dose and electrode montage that induce the most advantageous neurophysiological or behavioral effect on an individual basis. The current findings of a positive link between simulations and neuromodulation provide important groundwork for this aim.

Conflicts of interest

Declarations of interest: None.

Acknowledgements

This work was supported by the Bundesministerium für Bildung und Forschung (01GQ1424A). AT received support from Lundbeckfonden (R118-A11308) and Novo Nordisk Fonden by a synergy grant on Biophysically adjusted state-informed cortex stimulation (BASICS; NNF14OC0011413). The authors thank Angelica Sousa for help with data acquisition and Peter Jagd Sørensen for support in Matlab-based scripting.

Appendix A. Supplementary data

Supplementary data to this article can be found online at https://doi.org/10.1016/j.brs.2019.03.072.

References

[1] Polania R, Nitsche MA, Ruff CC. Studying and modifying brain function with non-invasive brain stimulation. Nat Neurosci 2018 Feb;21(2):174–87. https://doi.org/10.1038/s41593-017-0054-4.
[2] Kuo MF, Nitsche MA. Effects of transcranial electrical stimulation on cognition. Clin EEG Neurosci 2012;43(3):192–9.
[3] Krause B, Cohen Kadosh R. Not all brains are created equal: the relevance of individual differences in responsiveness to transcranial electrical stimulation. Front Syst Neurosci 2014;8:25.
[4] Stephens JA, Jones KT, Berryhill ME. Task demands, tDCS intensity, and the COMT val(158)met polymorphism impact tDCS-linked working memory training gains. Sci Rep 2017;7(1):13463.

[5] Opitz A, Paulus W, Will S, Antunes A, Thielscher A. Determinants of the electric field during transcranial direct current stimulation. Neuroimage 2015;109:140–50.
[6] Laakso I, Tanaka S, Mikkonen M, Koyama S, Sadato N, Hirata A. Electric fields of motor and frontal tDCS in a standard brain space: a computer simulation study. Neuroimage 2016;137:140–51.
[7] Kim JH, Kim DW, Chang WH, Kim YH, Kim K, Im CH. Inconsistent outcomes of transcranial direct current stimulation may originate from anatomical differences among individuals: electric field simulation using individual MRI data. Neurosci Lett 2014;564:6–10.
[8] Huang Y, Liu AA, Lafon B, Friedman D, Dayan M, Wang X, et al. Measurements and models of electric fields in the in vivo human brain during transcranial electric stimulation. Elife 2017;6.
[9] Hartwigsen G, Bergmann TO, Herz DM, Angstmann S, Karabanov A, Raffin E, et al. Modeling the effects of noninvasive transcranial brain stimulation at the biophysical, network, and cognitive level. Prog Brain Res 2015;222:261–87.
[10] Miranda PC, Mekonnen A, Salvador R, Ruffini G. The electric field in the cortex during transcranial current stimulation. Neuroimage 2013;70:48–58.
[11] Peterchev AV. Transcranial electric stimulation seen from within the brain. eLife 2017;6. e25812.
[12] Truong DQ, Adair D, Bikson M. Computer-Based Models of tDCS and tACS. In: Brunoni A, Nitsche M, Loo C, editors. Transcranial direct current stimulation in neuropsychiatric disorders: clinical principles and management. Cham: Springer International Publishing; 2016. p. 47–66.
[13] Saturnino GB, Antunes A, Thielscher A. On the importance of electrode parameters for shaping electric field patterns generated by tDCS. Neuroimage 2015;120:25–35.
[14] Cabral-Calderin Y, Williams KA, Opitz A, Dechent P, Wilke M. Transcranial alternating current stimulation modulates spontaneous low frequency fluctuations as measured with fMRI. Neuroimage 2016;141:88–107.
[15] Bungert A, Antunes A, Espenhahn S, Thielscher A. Where does TMS stimulate the motor cortex? Combining electrophysiological measurements and realistic field estimates to reveal the affected cortex position. Cerebr Cortex 2017;27(11):5083–94. New York, NY : 1991.
[16] Antonenko D, Schubert F, Bohm F, Ittermann B, Aydin S, Hayek D, et al. tDCS-induced modulation of GABA levels and resting-state functional connectivity in older adults. J Neurosci 2017;37(15):4065–73.
[17] Lindenberg R, Sieg MM, Meinzer M, Nachtigall L, Floel A. Neural correlates of unihemispheric and bihemispheric motor cortex stimulation in healthy young adults. Neuroimage 2016;140:141–9.
[18] Nitsche MA, Polania R, Kuo M-F. Transcranial direct current stimulation: modulation of brain pathways and potential clinical applications. Brain stimulation. John Wiley & Sons, Ltd; 2015. p. 233–54.
[19] Nitsche MA, Schauenburg A, Lang N, Liebetanz D, Exner C, Paulus W, et al. Facilitation of implicit motor learning by weak transcranial direct current stimulation of the primary motor cortex in the human. J Cogn Neurosci 2003;15(4):619–26.
[20] Polania R, Paulus W, Antal A, Nitsche MA. Introducing graph theory to track for neuroplastic alterations in the resting human brain: a transcranial direct current stimulation study. Neuroimage 2011;54(3):2287–96.
[21] Bachtiar V, Near J, Johansen-Berg H, Stagg CJ. Modulation of GABA and resting state functional connectivity by transcranial direct current stimulation. Elife 2015;4. e08789.
[22] Stagg CJ, Bachtiar V, Amadi U, Gudberg CA, Ilie AS, Sampaio-Baptista C, et al. Local GABA concentration is related to network-level resting functional connectivity. Elife 2014;3. e01465.
[23] Stagg CJ, Best JG, Stephenson MC, O'Shea J, Wylezinska M, Kincses ZT, et al. Polarity-sensitive modulation of cortical neurotransmitters by transcranial stimulation. J Neurosci 2009;29(16):5202–6.
[24] Kim S, Stephenson MC, Morris PG, Jackson SR. tDCS-induced alterations in GABA concentration within primary motor cortex predict motor learning and motor memory: a 7 T magnetic resonance spectroscopy study. Neuroimage 2014;99:237–43.
[25] Lindenberg R, Nachtigall L, Meinzer M, Sieg MM, Floel A. Differential effects of dual and unihemispheric motor cortex stimulation in older adults. J Neurosci 2013;33(21):9176–83.
[26] Meinzer M, Lindenberg R, Darkow R, Ulm L, Copland D, Floel A. Transcranial direct current stimulation and simultaneous functional magnetic resonance imaging. JoVE : JoVE 2014 Apr;27(86). https://doi.org/10.3791/51730.
[27] Watson C, Clark CM, Tellegen A. Development and validation of brief measures of positive and negative affect: the PANAS scales. J Personal Soc Psychol 1988;54:1063–70.
[28] Poreisz C, Boros K, Antal A, Paulus W. Safety aspects of transcranial direct current stimulation concerning healthy subjects and patients. Brain Res Bull 2007;72(4–6):208–14.
[29] Yousry TA, Schmid UD, Alkadhi H, Schmidt D, Peraud A, Buettner A, et al. Localization of the motor hand area to a knob on the precentral gyrus. A new landmark. Brain 1997;120(Pt 1):141–57.
[30] Gruetter R. Automatic, localized in Vivo adjustment of all first-and second-order shim coils. Magn Reson Med 1993;29(6):804–11.
[31] Gruetter R, Tkac I. Field mapping without reference scan using asymmetric echo-planar techniques. Magn Reson Med 2000;43(2):319–23.
[32] Mescher M, Merkle H, Kirsch J, Garwood M, Gruetter R. Simultaneous in vivo spectral editing and water suppression. NMR Biomed 1998;11(6):266–72.
[33] Edden RA, Intrapiromkul J, Zhu H, Cheng Y, Barker PB. Measuring T2 in vivo with J-difference editing: application to GABA at 3 Tesla. J Magn Reson Imaging : JMRI 2012;35(1):229–34.
[34] Provencher SW. Estimation of metabolite concentrations from localized in vivo proton NMR spectra. Magn Reson Med 1993;30(6):672–9.
[35] Stagg CJ. Magnetic Resonance Spectroscopy as a tool to study the role of GABA in motor-cortical plasticity. Neuroimage 2014;86:19–27.
[36] Mullins PG, McGonigle DJ, O'Gorman RL, Puts NA, Vidyasagar R, Evans CJ, et al. Current practice in the use of MEGA-PRESS spectroscopy for the detection of GABA. Neuroimage 2014;86:43–52.
[37] Whitfield-Gabrieli S, Nieto-Castanon A. Conn: a functional connectivity toolbox for correlated and anticorrelated brain networks. Brain Connect 2012;2(3):125–41.
[38] Behzadi Y, Restom K, Liau J, Liu TT. A component based noise correction method (CompCor) for BOLD and perfusion based fMRI. Neuroimage 2007;37(1):90–101.
[39] Calhoun VD, Liu J, Adali T. A review of group ICA for fMRI data and ICA for joint inference of imaging, genetic, and ERP data. Neuroimage 2009;45(1 Suppl): S163–72.
[40] Erhardt EB, Rachakonda S, Bedrick EJ, Allen EA, Adali T, Calhoun VD. Comparison of multi-subject ICA methods for analysis of fMRI data. Hum Brain Mapp 2011;32(12):2075–95.
[41] Calhoun VD, Adali T, Pearlson GD, Pekar JJ. A method for making group inferences from functional MRI data using independent component analysis. Hum Brain Mapp 2001;14(3):140–51.
[42] Thielscher A, Antunes A, Saturnino GB. Field modeling for transcranial magnetic stimulation: a useful tool to understand the physiological effects of TMS?. In: Conference proceedings : annual international conference of the IEEE engineering in medicine and biology society IEEE engineering in medicine and biology society annual conference 2015; 2015. p. 222–5.
[43] Windhoff M, Opitz A, Thielscher A. Electric field calculations in brain stimulation based on finite elements: an optimized processing pipeline for the generation and usage of accurate individual head models. Hum Brain Mapp 2013;34(4):923–35.
[44] Attene M. A lightweight approach to repairing digitized polygon meshes. Vis Comput 2010;26(11):1393–406.
[45] Geuzaine C, Gmsh Remacle J-F. A 3-D finite element mesh generator with built-in pre- and post-processing facilities. Int J Numer Methods Eng 2009;79(11). 1097-0207.
[46] Thielscher A, Opitz A, Windhoff M. Impact of the gyral geometry on the electric field induced by transcranial magnetic stimulation. Neuroimage 2011;54(1):234–43.
[47] Bindman LJ, Lippold OC, Redfearn JW. The action of brief polarizing currents on the cerebral cortex of the rat (1) during current flow and (2) in the production of long-lasting after-effects. J Physiol 1964;172:369–82.
[48] Rahman A, Lafon B, Parra LC, Bikson M. Direct current stimulation boosts synaptic gain and cooperativity in vitro. J Physiol 2017;595(11):3535–47.
[49] Verbeke G, Molenberghs G. Linear mixed models for longitudinal data. New York: Springer; 2000.
[50] Bachtiar V, Johnstone A, Berrington A, Lemke C, Johansen-Berg H, Emir U, et al. Modulating regional motor cortical excitability with non-invasive brain stimulation results in neurochemical changes in bilateral motor cortices. J Neurosci 2018 Aug 15;38(33):7327–36. https://doi.org/10.1523/JNEUROSCI.2853-17.2018.
[51] Barron HC, Vogels TP, Emir UE, Makin TR, O'Shea J, Clare S, et al. Unmasking latent inhibitory connections in human cortex to reveal dormant cortical memories. Neuron 2016;90(1):191–203.
[52] Hess G, Aizenman CD, Donoghue JP. Conditions for the induction of long-term potentiation in layer II/III horizontal connections of the rat motor cortex. J Neurophysiol 1996;75(5):1765–78.
[53] Trepel C, Racine RJ. GABAergic modulation of neocortical long-term potentiation in the freely moving rat. Synapse (N Y) 2000;35(2):120–8.
[54] Zimerman M, Nitsch M, Giraux P, Gerloff C, Cohen LG, Hummel FC. Neuroenhancement of the aging brain: restoring skill acquisition in old subjects. Ann Neurol 2013;73(1):10–5.
[55] Amadi U, Ilie A, Johansen-Berg H, Stagg CJ. Polarity-specific effects of motor transcranial direct current stimulation on fMRI resting state networks. Neuroimage 2014;88:155–61.
[56] Sehm B, Kipping J, Schafer A, Villringer A, Ragert P. A comparison between uni- and bilateral tDCS effects on functional connectivity of the human motor cortex. Front Hum Neurosci 2013;7:183.
[57] Opitz A, Yeagle E, Thielscher A, Schroeder C, Mehta AD, Milham MP. On the importance of precise electrode placement for targeted transcranial electric stimulation. Neuroimage 2018;181:560–7.
[58] Jacobson L, Koslowsky M, Lavidor M. tDCS polarity effects in motor and cognitive domains: a meta-analytical review. Exp Brain Res 2012;216(1):1–10.
[59] Mikkonen M, Laakso I, Sumiya M, Koyama S, Hirata A, Tanaka S. TMS motor thresholds correlate with TDCS electric field strengths in hand motor area. Front Neurosci 2018;12:426.
[60] Goksu C, Hanson LG, Siebner HR, Ehses P, Scheffler K, Thielscher A. Human in-vivo brain magnetic resonance current density imaging (MRCDI). Neuroimage 2018;171:26–39.
[61] Spitzer M, Wildenhain J, Rappsilber J, Tyers M. BoxPlotR: a web tool for generation of box plots. Nat Methods 2014;11(2):121–2.